Proposal of Density and Electrostatic Potential Fluctuation Measurements in the Madison Symmetric Torus with a Heavy Ion Beam Probe

Jianxin Lei

ECSE Department, Rensselaer Polytechnic Institute, Troy, NY 12180

July 15, 1999

ABSTRACT

A 200 keV heavy ion beam probe (HIBP) system is being installed on the Madison Symmetric Torus (MST) reversed field pinch (RFP). Measurements of electron density fluctuations and electrostatic potential fluctuations in MST are proposed here. For the first time particle transport induced by electrostatic field fluctuations in the core region of MST can be measured through the simultaneous measurement of electron density fluctuations $\tilde{n_e}$, electrostatic potential fluctuations $\tilde{\phi}$, and their wavenumbers. A Proca Green type electrostatic energy analyzer will be used to measure plasma fluctuations at two or three nearby sample locations. Wavenumber information is derived from the phase shift between sample volumes. A newly designed complex sweep plate system for both primary and secondary beam lines has been installed and will provide radial scanning of the beam probe. Issues such as finding sample volume locations, wavenumber measurements, correlation between fluctuation signals, energy transport due to fluctuations, and theoretical explanations of the observed fluctuations will be addressed in this study.

Contents

1 INTRODUCTION

The Reversed Field Pinch (RFP) is an attractive alternative path to fusion. The RFP belongs to the class of magnetic confinement configurations which are driven towards a state of "minimum energy" by internal dynamos (turbulence driven). Advantages of RFPs include high power density, less demanding magnet technology and a stable, natural minimum energy state plasma [1] [2] [3]. One of the major obstacles for the RFP as well as for other configurations is that observed particle and energy transport are anomalous and are much larger (two orders of magnitude) than classical and neo-classical predictions [4] [5].

Various fluctuations existing in a plasma have long been recognized to be responsible for the anomalous transport [7]. Fluctuations in electron density, electrostatic potential, magnetic field, electron temperature, particle velocity, and current density have been observed. Measurements and correlations between these fluctuations will provide information about transport driven by them, and help people to find ways to reduce transport and increase confinement.

Heavy ion beam probes (HIBP) have been used on a host of magnetically confined machines to measure eletrostatic potential [8] [9], electrostatic potential fluctuations [10] [11], electron density [12] [14], density fluctuations [10] [13] [15], magnetic vector potential [12], electron temperature [16] [17], and magnetic vector potential fluctuations [18].

Particle flux due to electrostatic fluctuations is given by $\Gamma =< \tilde{n_e} \tilde{v_E} >$, where $\tilde{v_E}$ is the $\mathbf{E} \times \mathbf{B}$ velocity fluctuation. An HIBP measures this transport through the simultaneous

measurement of electron density fluctuations and electrostatic potential fluctuations at two nearby sample volumes. In these measurements, the correlations and phase shift between the two measurements as well as the plasma wavenumber are important factors in determining Γ [19]. (Measurement of the electron energy transport needs additional information about $\tilde{Te}$ from other diagnostics). Such measurements are made in MST by using Langmuir probes, but only in the edge region during low density and low current plasmas. A heavy ion beam probe can make measurements much further into the core plasma. A nearly complete radial scan can be obtained by changing the beam's entrance angle and energy.

A 200 keV heavy ion beam probe is being installed on MST to measure the equilibrium potential profile, electrostatic potential fluctuations, electron density fluctuations, magnetic field fluctuations, and transport caused by fluctuations. This beam probe system will use a Proca Green type electrostatic energy analyzer to make measurements at 2 or 3 points simultaneously. The analyzer is a modified version of the one used on the 500 keV TEXT HIBP. A major difference between this system and previous ones is a newly designed, complex sweep plate system used on both primary and secondary beamlines to give a radial scan of the plasma.

The proposed thesis will focus on measurement of electron density fluctuations and electrostatic potential fluctuations in the MST plasma. On the experimental side, this not only provides MST with a powerful diagnostic tool to measure strong turbulent features in the MST plasma, but also will provide useful information about experiments pursuing various methods of improving confinement by reducing fluctuation driven transport. On the theoretical side, the data from these measurements will help identifing the cause of $\tilde{E}$ in the MST

plasma which is still unknown. It will also inspire theoretical work on the role of electrostatic potential fluctuations [20]. Finally, it will shed some light on the investigation of dynamo mechanisms, various predictions about the level of electrostatic potential and density fluctuations, and turbulence induced anomalous transport. Issues such as finding sample volume locations, wavenumber measurements, correlation between fluctuation signals, energy transport due to fluctuations, and theoretical explanations of the observed fluctuations will be addressed in this study.

In section 2, the importance of $\tilde{n_e}$ and $\tilde{E}$ measurements on MST with HIBP will be discussed. Section 3 will show a brief description of MST and the HIBP designed for MST. In order to analyze fluctuation features, broadband spectral information as well as correlations, phase, and time evolution are needed. In section 4, transform methods to analyze the fluctuating data will be given. In the last section, I will discuss some challenges we will face with MST HIBP measurements. Suggestions to overcome those problems will be discussed.

2 IMPORTANCE OF $\tilde{n_e}$ AND $\tilde{\phi}$ MEASUREMENT IN MST

A focus of the MST has been the measurement of fluctuations and in particular, the transport directly driven by fluctuations [4]. Many fluctuations and fluctuations induced transport measurements have been done in the MST. The present set of MST diagnostics consists largely of single point or single chord measurements, with profiles of a few quantities available on a discharge -to-discharge basis [4]. Table I summarizes those major diagnostics currently being used to measure fluctuation quantities.

Table I: Major Fluctuations Diagnostics on the MST

Name	Measurement
FIR	$\tilde{n_e}$ (11 chords)
Magnetic Coil Array	$\tilde{B}$ (at the chamber)
Langmuir Probes	$\tilde{n_e}, \tilde{T_e}, \tilde{E}$ (at the edge)
Current Density Probes	$\tilde{j}$ (at edge)
Ion Dynamic Spectroscopy	Impurity ion $\tilde{v}$ (chord view)

For example, magnetic field fluctuations that are driven by resistive tearing modes have been measured in the $r/a > 0.75$ region to be responsible for the anomalous particle and energy transport inside the reversal surface by correlating parallel current density fluctuations and parallel electron heat flux with radial magnetic field fluctuations respectively [21]. Electrostatic fluctuation driven particle and energy transport at the edge ($r/a \geq 0.92$) have also been measured. These fluctuations are responsible for the extreme edge anomalous particle transport, but are too small to explain its energy loss [26]. Direct measurement of chord

averaged velocity fluctuations of impurity ions have been done with Doppler spectroscopy (IDS) [27] [28]. Electron density fluctuations have been measured by FIR [29]. Current density fluctuations are measured with inserted probe coils. [5] [30]

Most transport related fluctuations measurement have been done at the edge of the plasma ($r/a \sim> 0.75$). The core region transport from fluctuations remains largely undiagnosed. If $\tilde{n_e}$, $\tilde{E}$, $\tilde{T_e}$, and their correlations could be measured throughout the plasma volume, the electrostatic components of the various fluctuation-driven fluxes could be determined [31].

HIBP can extend localized $\tilde{n_e}$ and $\tilde{E}$ measurements much further into the core where they have never been measured in MST, and be used over a broader range of plasma parameters than is possible with Langmuir probes. Thus HIBP measurements will yield more insight into the turbulent processes inside the plasma.

With the information provided by the HIBP, not only the edge fluctuation data from Langmuir probes can be cross checked (HIBP is a complementary measurement to Langmuir probes at the edge), but also the residual transport caused by electrostatic field fluctuations can be derived once magnetic fluctuation levels been suppressed [4]. Thus the importance of $\tilde{E}$ induced transport can be addressed.

It has long been understood that the magnetic fluctuations are caused by resistive MHD modes (tearing modes) driven by j/B gradients in the MST. But a major unknown is the cause of electrostatic fluctuations, although people believe $\tilde{E}$ may be coupled to tearing modes. The HIBP can be used as an experimental way to check conjectures about their

origin [4].

The MST group has proposed a theoretical investigation of electrostatic fluctuations which includes a detailed comparison to experimental measurements. The investigation will have four components [4]: analytic calculation of the characteristics and saturated amplitudes of fluctuations which are suspected to be important (such as interchange modes), use of flux tube computation of electrostatic turbulence such as has been developed in the tokamak context, evaluation of electrostatic fluctuations coupled to the large-scale resistive MHD core-resonant fluctuations, and treatment of the edge as a self-organized critical (SOC) state. The strong core turbulence may drive the edge into a SOC, perhaps accounting for the commonality of fluctuation properties in the RFP, tokamak, and stellarator. This approach could explain why particular modes have not been successful in explaining edge turbulence.

Detailed discussion of these models are beyond the scope of this proposal. Each of those models may treat only one or two aspects of a specific plasma which can run over a broad range of parameters. Therefore measurement of these fluctuation levels under different conditions, at different positions can provide a lot of information for the developement of theories. The most important thing is to reduce fluctuation levels and transport, and to increase confinement. And this can best be done with guidance from theoretical work. One such successful example is pulse poloidal current drive (PPCD) in which inductively driven edge current increases confinement and reduces fluctuation levels. The current drive stabilizes resistive tearing modes driven by j/B gradients (inside the reversal surface of $r/a = 0.85$) which are responsible for large magnetic fluctuations and magnetic island overlap which in turn causes large core transport.

This proposal will focus only on the electrostatic fluctuation induced transport, which means simultaneous measurement of $\tilde{n}$ and $\tilde{\phi}$ at two nearby sample volumes. Wavenumbers and correlations between fluctuation signals are obtained with these measurements. Also, a comparison of $\tilde{v}_r$ derived from $\tilde{\mathbf{E}} \times \mathbf{B}$ of HIBP measurements and that from CHERS (Rutherford) measurements will be studied.

To summarize, the MST HIBP can provide localized fluctuation measurements at almost all radii for a broad range of plasma conditions, can address $\tilde{E}$ induced transport, and can enlighten the theoretical work on the cause of $\tilde{E}$ and its role in RFPs. In addition, this measurement will enrich the understanding of turbulent transport in different magnetically confined plasmas.

3 MST AND HIBP FOR MST

3.1 MST

The MST is a reversed field pinch toroidal configuration. Its minor radius of 52 cm and major radius of 150 cm makes it one of the largest RFPs in the world. (See figure 1). Unlike tokamaks and stellarators the RFP magnetic field structure is not simply dominated by the toroidal magnetic field. In fact, the toroidal and poloidal field components are roughly the same order of magniude (Figure 2). The name RFP arises because the toroidal magnetic field at the edge reverses direction relative to the interior. This configuration is produced by a self relaxation process of the plasma. Although the reason for this relaxation process is not exactly known, the process itself has been theoretically described by Taylor [32] and is attributed to the attainment of a minimum energy state by the plasma, subject to the constraint that the total helicity $\int \mathbf{A} \cdot \mathbf{B} dv$ be conserved. Another interesting feature of the RFP is the dynamo mechanism. While this mechanism is the chief reason behind RFP field sustainment, it is also the cause of turbulent magnetic fluctuations in this type of configuration. The MST operates under a variety of discharge conditions. There are basically two types of operating modes on MST. One is the standard discharge which is characterized by high fluctuation amplitude levels and is highly reproducible from shot to shot. The other type has reduced fluctuations and increased confinement due to current profile control. These discharges are called (a) pulse poloidal curent drive (PPCD), (b) enhanced confinement (EC), and (c) electrostatic bias [22]. Figure 3 shows the Te difference between standard and PPCD discharges in MST. From the perspective of a heavy ion beam

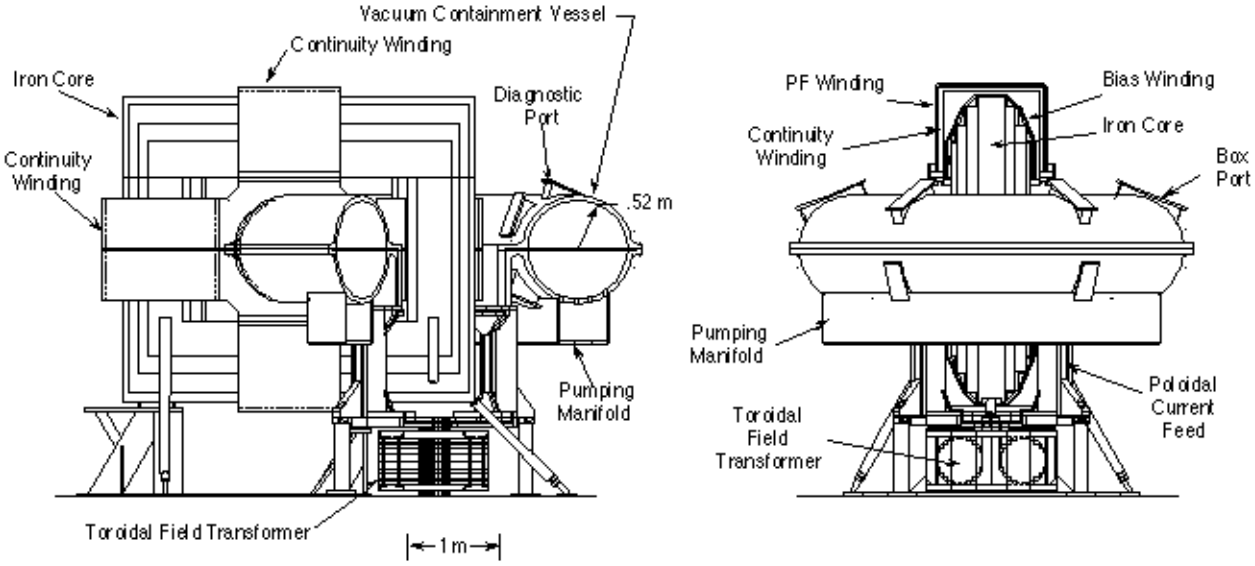

Figure 1: Schematic view of MST

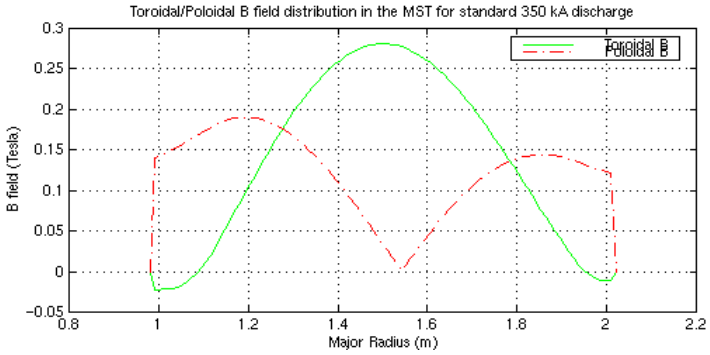

Figure 2: Magnetic field profile in MST

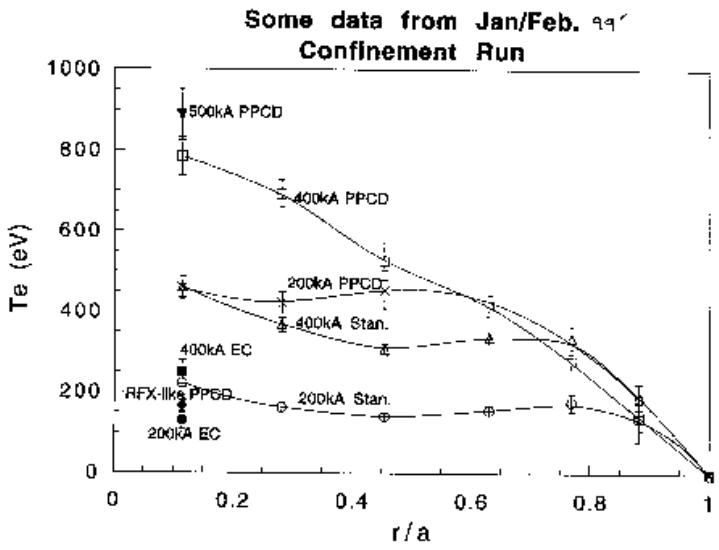

Figure 3: Te profile during PPCD and standard discharge

probe, a reproducible discharge will be ideal for calibration purposes. But a low $\tilde{B}$ will let us track the beam trajectory more confidently. I plan to study both standard and PPCD discharge cases with HIBP, so that the importance of electrostatic fluctuation induced transport can be addressed under different discharges.

3.2 HIBP for the MST

The schematic of the MST HIBP system is shown in figure 4. This heavy ion beam system consists of: A 200 keV Peabody accelerator system previous used on ATF [38] and ISX-B [24], electrostatic sweep systems, a modified Proca-Green electrostatic energy analyzer [25] previously used with the 500 keV TEXT HIBP, control systems, data acquisition systems, and other auxiliary systems. The accelerator has multiple power suppliers and a thermionic ion source. Na^+, K^+, and Li^+ ions will be used in these experiments. The electrostatic sweep

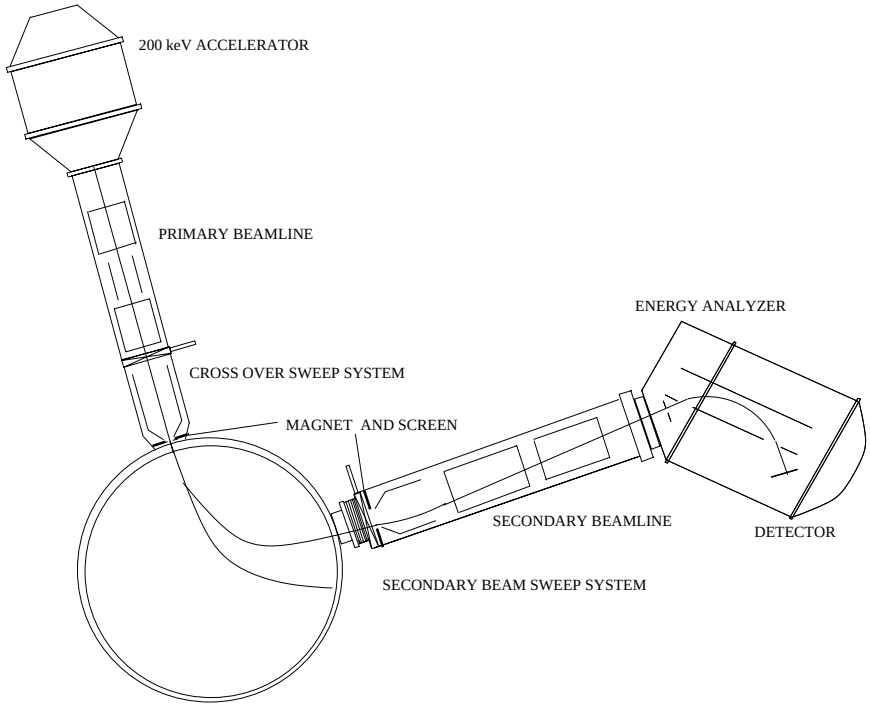

Figure 4: Schematic of MST HIBP [23]

system includes 4 pairs of primary and 3 pairs of secondary sweep plates [33]. In the primary beamline, 2 pairs of plates in both poloidal and toroidal directions form a ± 20 degrees and ± 5 degrees crossover sweep in each direction. In the secondary beamline, one pair of plates in the poloidal direction directs the secondary ion beam into the analyzer entrance slit with a ± 3 degree entrance angle range, while 2 pairs of toroidal plates can collimate the beam into the analyzer with a 0° out of plane angle. The sweep systems are driven by fourteen 4-20 kV Trek power supplies which have slew rates between $35 - 100 V/\mu S$. A detailed sweep plate design is available online [40]. The electrostatic energy analyzer has 3 entrances to enable wavenumber measurements. It has been modified from its original configuration to reduce UV loading effects.

4 FLUCTUATION MEASUREMENTS AND DATA ANALYSIS

4.1 General Principles of HIBP

As shown in figure 5, a heavy ion beam probe diagnostic injects a continuous, monoenergetic, focussed beam of singly charged ions into a plasma with suitably positioned analyzer to measure the ion beam or beam particles with higher charge states when they exit the plasma. The singly charged or 'primary' beam comes from an electrostatic ion accelerator that is

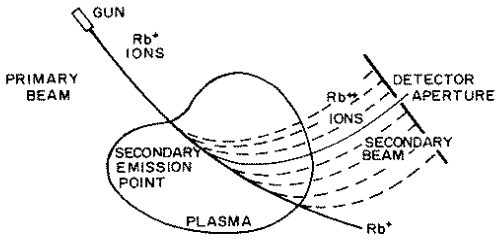

Figure 5: Principle of a heavy ion beam probe

focussed and steered with electrostatic sweep plates. The ions used are usually type IA elements from the periodic table (Li, Na, K, Rb, Cs) or Tl and are considered 'heavy' compared to the plasma particles. The primary beam particles of mass, m_b, and energy, E_b, enter the $\mathbf{B}$ field from injection point, $\mathbf{0}$, and change direction mainly due to Lorentz force interaction with B_t and B_θ. Interaction with B_θ causes a deflection out of the plane of figure 5 and is more important on MST than most previous HIBP experiments. All along the primary beam trajectory in the plasma, the beam particles are ionized to higher charge states mainly through electron impact ionization. There is virtually no net momentum transfer due to the large mass difference, so the higher charge state particles begin parallel to the primary beam,

but they soon diverge due to a larger Lorentz force. From a certain localized sample volume or ionization position, **i**, on the primary beam, a Proca-Green energy analyzer intercepts a portion of net charge +2, 'secondary' particles to measure the current on a set of split detector plates as shown in figure 6. By varying E_b and sweep plate settings, a large portion of a plasma can be scanned.

Different measurements of plasma parameters result from the combination of the individual split plate signals, $I_{top,left}$, $I_{top,right}$, $I_{bottom,left}$, and $I_{bottom,right}$. The sum of the four split plate signals yields the total secondary beam current, $I_{sec} = I_{sum} = I_{top,left} + I_{top,right} + I_{bottom,left} + I_{bottom,right}$, which can be related to local n_e and $\tilde{n_e}$. The difference signal, $I_{diff} = I_{top,left} + I_{top,right} - I_{bottom,left} - I_{bottom,right}$, is related to local ϕ and $\tilde{\phi}$. The $\tilde{n_e}$, ϕ, and $\tilde{\phi}$ measurements will be derived in the following subsections.

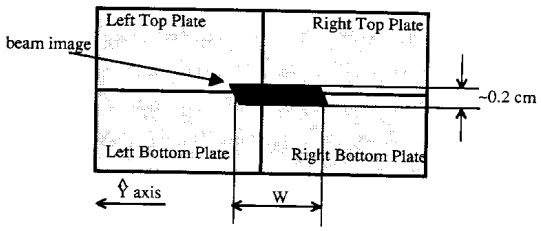

Figure 6: View of Beam Image on the Split Plates [34]

4.2 Density fluctuation measurement

The secondary signal i_s impinging on the detector plates is proportional to the local density n_e

$$i_s \propto n_e n_b < \sigma_i v >$$

where $< \sigma_i v >$ is the average ionization rate of primary beam ions by plasma electrons which depends on the plasma temperature T_e, and n_b is the local beam density [35]. As T_e in the core of MST is several hundred eV, $< \sigma_i v >$ is almost constant for the type of ions we are going to use. Hence the relative fluctuation in the collected secondary signal gives the relative density fluctuation level at the measurement volume:

$$\frac{\tilde{i_s}}{< i_s >} = \frac{i_s - < i_s >}{< i_s >} = \frac{\tilde{n_e}}{< n_e >} \tag{1}$$

where $< ... >$ denotes averaged values.

4.3 Electric field fluctuation measurement

The plasma potential at the sample volume position can be obtained from :

$$\phi_{sv} = \frac{W_d - W_i}{q_s - q_p} \tag{2}$$

where W_d is the beam energy at the detector, W_i is the beam initial energy, q_s and q_p are secondary and primary ions charge state. The beam energy W_d at the detector is measured by using [36]:

$$W_d = q_s V_A \left\{ G(\theta_I, \alpha) + F(\theta_I, \alpha) \frac{i_U - i_L}{i_U + i_L} \right\} \tag{3}$$

where V_A is voltage on the analyzer anode, i_U and i_L are the currents on the upper and lower plates, $G(\theta_I, \alpha)$ is called the 'ideal gain function' and is given by:

$$G(\theta_I, \alpha) = \frac{X_D tan\theta_I - Y_D}{4dsin^2\theta_I cos^2\alpha}$$

$F(\theta_I, \alpha)$ is called the 'ideal off-line processing function', and is given by:

$$F(\theta_I, \alpha) = \frac{w(sin\theta + cos\theta tan\theta_I)}{8dsin^2\theta_I cos^2\alpha}$$

θ_I is the poloidal angle (see figure 7), and α is the toroidal (out of plane) injection angle at the entrance slit plane of the analyzer. From (2) and (3), one can calculate the potential

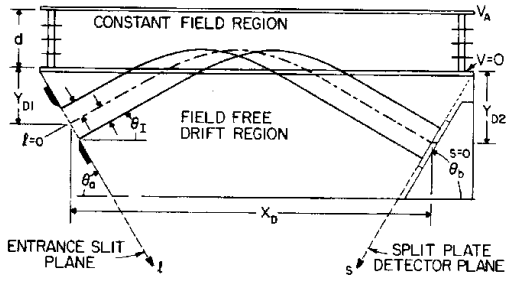

Figure 7: Schematic drawing of the Proca-Green parallel plate energy analyzer

fluctuation signal at the sample volume [36]:

$$\tilde{\phi} = \frac{q_s}{q_s - q_p} V_A F(\theta_I) \Delta((i_U - i_L)/(i_U + i_L)) \tag{4}$$

where $\Delta((i_U - i_L)/(i_U + i_L))$ is the fluctuation in the difference to sum ratio.

4.4 Wavenumber (average k) measurement

The fluctuating electric field $\tilde{E}$ is derived from $\tilde{E} = -ik\tilde{\phi}$, where k is the wavenumber of the fluctuation. The HIBP for the MST has the ability to simultaneously measure two nearby sample volumes (with multiple entrance slits on the analyzer). The phase shift Δ_p between these two signals and the distance between the two sample positions d will tell us the average wavenumber $\bar{k}$

$$\bar{k} = \frac{\Delta_p}{d}$$

Note, this is just the 'average k' along the direction connecting these two sample volumes when multiple modes are present [31]. The upper limit for k measurement is determined

by the sample volume and is usually $< 5cm^{-1}$. The sample volume size is determined by the beam size, beam divergence, magnetic configuration, sample volume location, and the entrance slit width. Usually, we want to focus the beam as small as possible using the accelerator optics. The width of the entrance slit can not be too small in order to get proper signal levels. The distance between entrance slits is usually fixed.

There are two factors that are going to influence our k measurement. One is that the poloidal magnetic field is comparable to the toroidal magnetic field. This causes a toroidal separation of the sample volumes and the measured k will usually be a combination of k in toroidal, poloidal, and radial directions. The k direction needed for transport measurements is a combination of poloidal and toroidal components. It is probably not possible to isolate one component. The second factor is that the secondary sweep system will complicate wavenumber measurements in our experiment. I'll discuss this issue in the next section.

4.5 Electrostatic fluctuation induced particle and energy transport

Particle flux driven by fluctuations is given by:

$$\Gamma^f = \Gamma^f_E + \Gamma^f_b \tag{5}$$

where

$$\Gamma^f_E = \frac{< \tilde{E_\perp} \tilde{n} >}{B} \tag{6}$$

is particle flux induced by electrostatic fluctuations, and Γ^f_b is particle flux induced by magnetic fluctuations [31]. Energy flux driven by fluctuations is:

$$Q^f = Q^f_E + Q^f_b \tag{7}$$

where

$$Q_E^f = \frac{3}{2}k_b n\frac{<\tilde{E_\perp}\tilde{T}>}{B} + \frac{3}{2}k_b T\frac{<\tilde{E_\perp}\tilde{n}>}{B} \tag{8}$$

is energy flux caused by electrostatic fluctuations, and Q_b^f is energy flux caused by magnetic fluctuations. In equation (8), k_b is Boltzmann constant. From above, we can see that an HIBP can measure $\tilde{E}$ induced particle flux directly by correlating $\tilde{E}$ and $\tilde{n}$. But in order to get energy flux, temperature information from other diagnostics is needed, although correlation with HIBP measurements will probably be very difficult.

There are two methods that will be used to calculate correlations between two signals: one is in the time domain with statistical analysis, the second is in the frequency domain with discrete Fourier transforms (DFT). The two methods give similar ensembled averaged results, with each concentrating on different signal features.

In the time domain, of primary interest for the HIBP data is the cross-correlation of two signals, $X_1(t)$ and $X_2(t)$, defined by:

$$\rho_{12}(\tau) = \frac{R_{12}(\tau)}{[R_{11}(0)R_{22}(0)]^{1/2}} \tag{9}$$

where $R_{12}(\tau)$ is called the cross-covariance of X_1 and X_2, and is given by

$$R_{12}(\tau) = \langle (X_1(t) - \bar{X_1})(X_2(t+\tau) - \bar{X_2}) \rangle$$

where $< ... >$ denotes an expectation value [36]. Cross-correlation can tell whether there are two modes present in the plasma.

In the frequency domain, Fourier transforms tell the spectral character of the turbulence. The phase shift at any frequency between two signals is also derived by the DFT, thus

wavenumber and phase speed can be calculated. The DFT is used for many fluctuation measurements, particularly broadband turbulence. The HIBP experiments use the coherence and phase with two different combinations of signals. The first combination is correlating two signals (which measure the same plasma parameter) from two nearby sample volumes. The second combination is correlating two signals (which measure different plasma parameters) from the same sample volume. If $S_1(f)$ and $S_2(f)$ are Fourier transforms of two signals, coherence is given by:

$$\gamma(f) = \frac{|P_{12}(f)|}{[P_1(f)P_2(f)]^{1/2}}$$

where $P_1(f)$ is autopower of $S_1(f)$, $P_2(f)$ is autopower of $S_2(f)$, and $P_{12}(f)$ is cross-power of $S_1(f)$ and $S_2(f)$ [36]. E. J. Powers [19] gave the electrostatic fluctuation induced particle flux as:

$$\begin{aligned} < \tilde{n}\tilde{v} > &= \frac{1}{B} < \tilde{n}\tilde{E} >= \frac{2}{B}\int_0^\infty k(\omega)|P_{n\phi}(\omega)|sin[\alpha_{n\phi}(\omega)]d\omega \\ &= \frac{2}{B}\int_0^\infty k(\omega)|\gamma_{n\phi}(\omega)|sin[\alpha_{n\phi}(\omega)][P_{nn}(\omega)P_{\phi\phi}(\omega)]^{1/2}d\omega \end{aligned} \tag{10}$$

where $\alpha_{n\phi}(\omega)$ is the phase difference between $\tilde{n}_e$ and $\tilde{\phi}$ signals, and the wavenumber spectrum $k(\omega)$ has to be derived from two point measurements.

Both methods will have important applications in our data analysis. But the time domain methods can't tell wavenumber information, while the DFT loses time features of any modes. In order to address time features in the highly unstationary signals in practice, the short term Fourier transform (STFT) is used. With the STFT, a proper window function is chosen (with experience) to cover separate time sections of a signal to locate specific features of the signal within that section. What kind of a window should be used? Narrow windows give good time resolution, but poor frequency resolution. Wide windows give good frequency

resolution, but poor time resolution. Furthermore, wide windows may violate the condition of stationarity. This can be very tricky and tedious. In addition, a leakage problem should be avoided.

4.6 Wavelet transform

Wavelet transforms are capable of providing a time-frequency representation of the signal, similar to the STFT above, but solve the problem of resolution differently [41].

Wavelet analysis is done in a similar way to the STFT analysis, in the sense that the signal is multiplied with a function, *the wavelet*, similar to the window function in the STFT, and the transform is computed separately for different segments of the time-domain signal. However, there are two main differences between the STFT and the wavelet transforms:
1. The Fourier transforms of the windowed signals are not taken, and therefore a single peak will be seen corresponding to a sinusoid, i.e., negative frequencies are not computed.
2. The width of the window is changed as the transform is computed for every single spectral component, which is probably the most significant characteristic of the wavelet transform.

The continuous wavelet transform is defined as follows

$$CWT_x^{\psi}(\tau, s) = \Psi_x^{\psi}(\tau, s) = \frac{1}{\sqrt{|s|}} \int x(t)\psi^*(\frac{t-\tau}{s})dt \tag{11}$$

As seen in the above equation , the transformed signal is a function of two variables, τ and s , the translation and scale parameters, respectively. $\psi(t)$ is the transforming function, and it is called the mother wavelet .

Wavelet transforms have been used on the MST to study the evolution of the velocity fluctuations over a sawtooth where the frequency spectrum has a strong time dependence [37]. I propose to apply wavelet transforms in the HIBP data analysis, with the hope to get some useful information about the evolution of the fluctuations.

5 CHALLENGING ISSUES FOR THE MST HIBP DIAGNOSTIC

The MST HIBP is designed specifically to work only for the MST (like previous machines). We have encountered many serious issues during the designing process, and we will encounter many problems during the experiments. Some are general to all HIBPs, but some are more specific to fluctuation measurements with the MST HIBP. The following discussion is not an attemp to cover all the issues that we may have. Also, we don't have firm answers to all the issues which can only be studied in detail later.

5.1 Sweep plate calibration issue

As sweep plates play an important role in the new HIBP system, calibration of it becomes essential to our measurement. Basically, there are two ways to do this:

1. Numerical methods:

(1) The finite element program Flux2D can solve a 2 dimentional Laplace equation. Flux3D can solve the 3D problem but requires much more computing time. In addition, it's almost impossible to get the same resolution with Flux3D as from Flux2D with present computer capabilities. Flux2D was used in previous HIBPs to derive sweep angles [12] [38]. Figure 8 shows the sweep angles in the primary sweep system in the poloidal direction calculated from Flux2D, as well as from our modified model which has been used in the sweep system design.

(2) The boundary charge method (BCM) can be used to calculate the field. We divide each

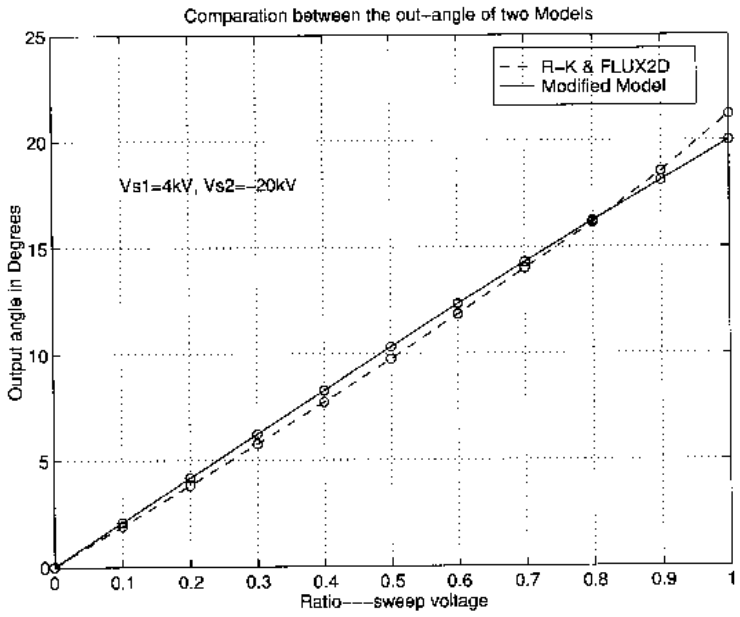

Figure 8: Sweep angles calculated from Flux2D and modified model

sweep plate into mesh grid elements and assume that the charge density on each element is uniform. The potential of a point $\mathbf{r}_i$ in the space is then [39]:

$$U_i = \frac{1}{4\pi\varepsilon_0} \sum_{j=1}^{N} \sigma_j \iint \frac{ds_j}{|\mathbf{r}_i - \mathbf{r}_j|} \tag{12}$$

where ε_0 is permittivity in vacuum, σ_j is the free charge density on element j, $\mathbf{r}_j$ is the center point of element j, and the integration is over the surface of each grid element, summation is over all elements 'N'. The charge density on each element is calculated by applying the above equation on each sweep plate's boundary. For a 3D problem with an open boundary as in our situation, the BCM method is more suitable than the finite element method. I will pursue this method and cross check it with Flux2D results.

2. In situ calibration: (primary sweep plates only)

(1) A set of detection wires will be positioned at the end of the primary beamline for measuring beam position. We can also use 'scrape off' on the 4 pairs of sweep plates in the

primary beamline to determine beam position (See figure 9).

(2) Primary beam detectors.

Single pin, multi-pin, cross-rod and rotary rod detectors have been placed at the bottom of the MST chamber opposite to the beam injection port through the pumping holes (see figure 10). Details are posted online [41]. In the radial direction, $\sim \pm 12^{\circ}$ sweep can be detected. In the toroidal direction, approximately 1° misalignments may be detected. Detectors at other places are positioned to monitor the beam during a discharge.

For the secondary sweep plates, only numerical methods can be used, since there is no way to shoot a primary beam with an accurately known injection angle into the secondary beamline.

5.2 Energy analyzer calibration issue

The calibration of the analyzer is most important for measurement of the plasma potential. One motivation of calibration is to find the inflection angle θ_{I0} of the ideal 'gain function' $G(\theta_I, \alpha)$ in the equation (3) of previous section. The best way to do this is shooting a singly charged ion beam into the analyzer with known beam energy. By adjusting voltage on the analyzer's anode and balancing up-and-down current on the detectors, 'gain' can be derived. Preliminary calibration has been done on RPI's test stand, and a gain curve achieved.

However, in situ calibration is also needed because the analyzer has been moved. This will present some difficulties in our case due to (1) uncertainties in the plasma produced

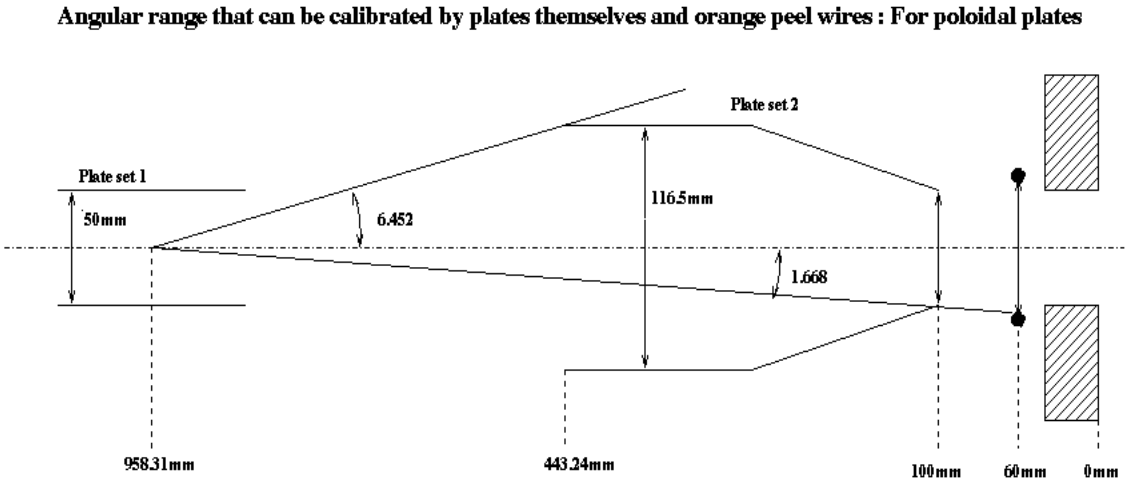

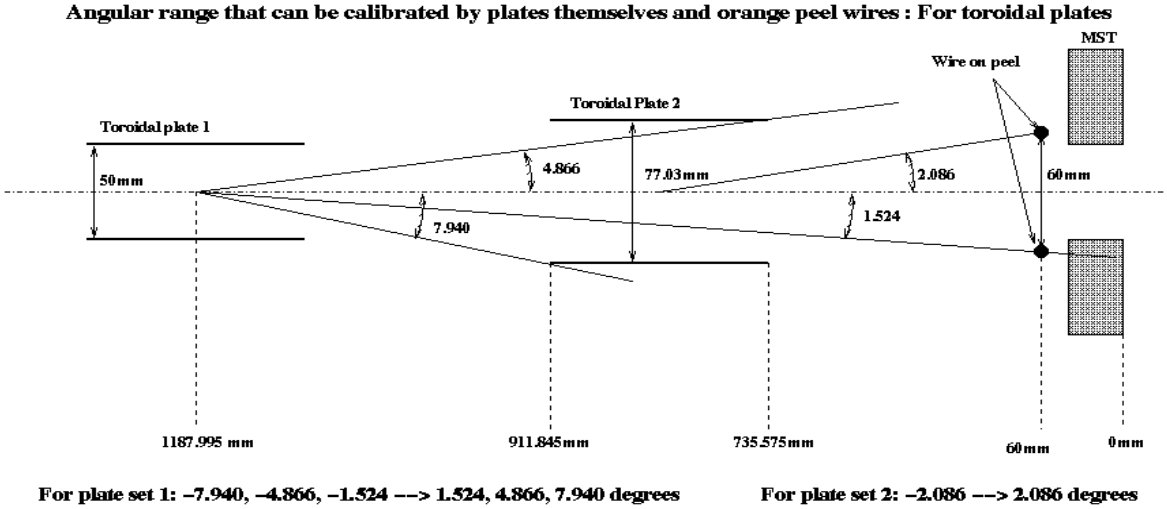

Figure 9: Sweep angles at some 'scrape off' points

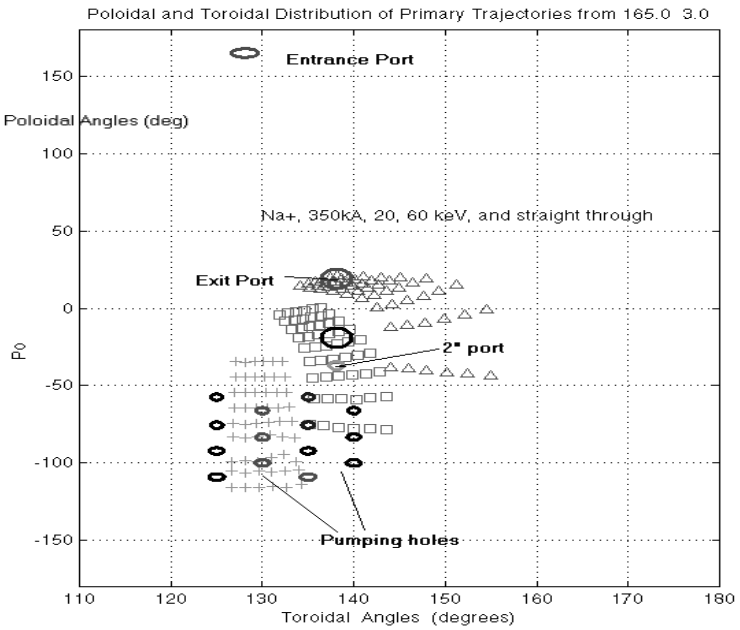

Figure 10: MST pumping holes, HIBP injection port and exit port, etc.

magnetic field, (2) high magnetic fluctuation levels ($\sim 1\%$), and a (3) short plasma lifetime. Recent calculations have shown that at some low energies ($\sim$ 20 keV for Na+), ion beams can reach the 4.5" exit port that is used for the HIBP (see figure 10). Therefore, there is a possibility that we can use singly charged sodium or lithium ions to calibrate the analyzer. I will take a further look at this possibility later.

An alternative way of calibration is using secondary charged ions. In his proposal of plasma potential measurement in the MST, Uday Shah has shown some details of this kind of calibration [43]. One unknown here is how the plasma potential will influence calibration in this way.

For both methods, (1) secondary sweep plates play an important role. We have to combine the sweep plates' voltage information and that of up-down, left-right current information on the detector plates in order to decide the incoming beam's positions and angles. At the

analyzer entrance plane, toroidal injection position and angle can be uniquely decided by voltages on the 2 pairs of toroidal sweep plates and left-right current on the detector plates. However, poloidal injection position and angle can not be uniquely decided, because we only have one pair of poloidal sweep plates in the secondary beamline. This can be partly solved if a slit or aperture is used in front of the 1st set of the sweep plates. (2) A large number of shots are needed in order to gradually accumulate enough information to derive the gain curve. Hence, shot to shot reproducibility is needed.

5.3 Sample volume location issue

If we assume that the trajectory of the diagnostic ion beam can be accurately decided in the HIBP's electrostatic optic system, then the exact location of the sample volume will be decided by the actual magnetic field distribution in the MST. In a RFP machine like MST, the magnetic field is partially generated by the plasma itself and only partially known. Therefore, how to locate the sample volumes is a great challenge for the MST HIBP.

In our HIBP design process, the magnetic equilibria field of the MST that has been used to calculate trajectories comes from a 2-D toroidal fit model. This model basically solves the Grad-Shavranov equation and self consistently maps the measured edge magnetic field (from pick up coils) and chord-averaged magnetic field (from FIR) to the whole poloidal cross section. We expect that for our measurement, case by case study of the magnetic field and trajectoies will be needed.

Despite the fact that the magnetic field is not very accurately known, the deviation from

the actual MST fields is not expected to drastically change the shape of the field profiles used in theoretical calculations, but rather the relative magnitudes of B_t and B_θ across the minor radii. The pre and post sawtooth models shown in figure 11 have both been used to calculate sample volumes in MST. If we hypothetically consider the two cases to represent the upper and lower limit of the magnetic fields, and use this for trajectory calculation, we see that this results in location uncertainties in sample volumes of about 10 cm or less in the core region (see figure 12).

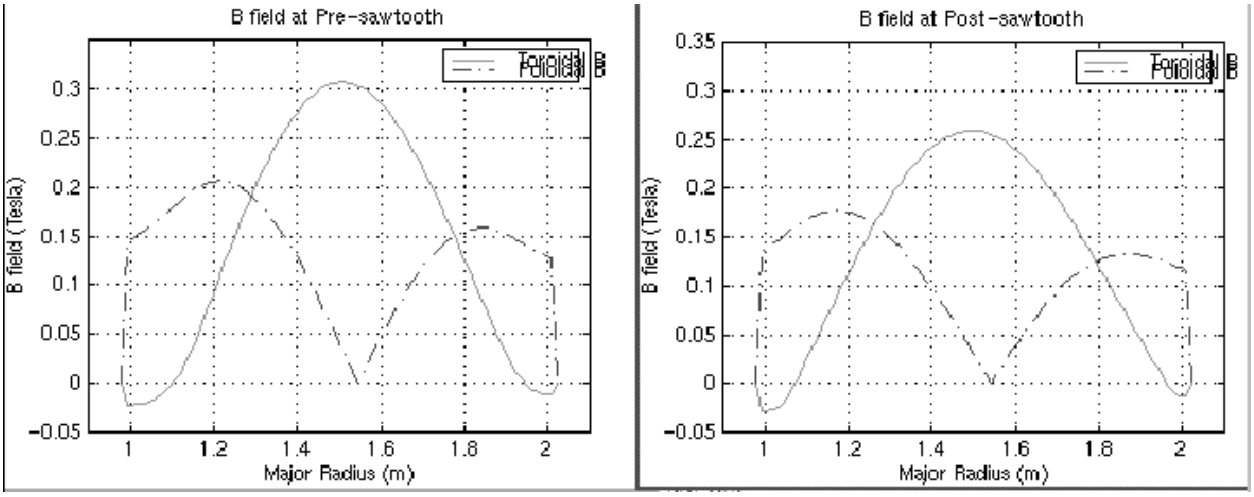

Figure 11: B field of MST at Pre and Post sawtooth

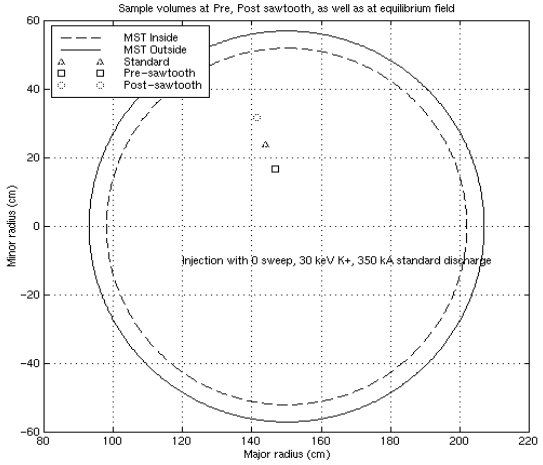

Figure 12: Sample volumes of MSTHIBP at Pre and Post sawtooth

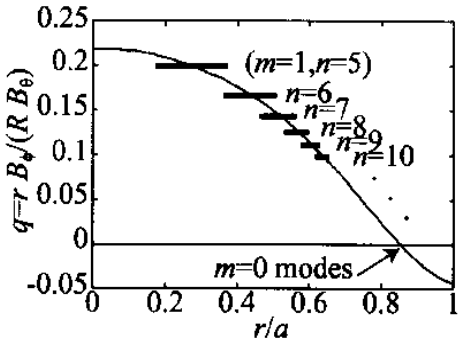

Figure 13: q profile and MHD modes

While uncertainties in sample volume locations due to relatively unknown magnetic fields is a big challenge, there are ways to reduce these errors. In Uday Shah's thesis proposal [43], some suggestions were proposed:

(1) Making use of the secondary signal's dependence on density $n_e(r)$ and temperature $T_e(r)$ profiles. But this will subject to the fairly uniform distribution of density and temperature within the reversal surface of the MST.

(2) Making use of the information that the dominant fluctuations in the MST are core resonant magnetic tearing modes centered around (poloidal) $m = 1$ and (toroidal) $n = 5, 6, 7$. Mode information will show up in the density spectrum. But this technique is limited because the modes overlap and have global properties. Figure 13 shows a typical q profile with relative sizes of islands sizes and positions.

(3) If it turns out that $\phi(r)$ in the core varies rather significantly over short distances, this can enable rather accurate determination of flux surfaces which can be compared to theory to yield sample volume position information.

As all the above methods have their shortcomings, we would suggest the B field model

mentioned previously to be our major tool to locate the sample volumes at different timing points. Cross checking with the density and temperature information, as well as dominant MHD mode caused fluctuation signals are needed for better location of the sample volumes.

5.4 Plasma/UV loading effect issue

The sweep plates play an important role in our newly designed HIBP system, and our design is based on an ideal case in which we expect the power supplies that drive those sweep plates can keep the output at the exact values we program. Because any power supply has a current limit, the voltage output of a power supply can drop to zero if this limit is exceeded. This becomes serious if there is plasma/UV loading present on the sweep plates, especially for those close to the MST ports. We have conducted a series of sweep plates tests since summer 1997. The results from these tests are summarized as following:

(1) Loading effect is plasma dominated, and very striking.

(2) The power supply can not hold its voltage under normal discharge conditions without any plasma suppression structures.

(3) Plasma loading effect is especially serious during sawtooth process.

(4) Negative driving works better than positive driving.

(5) Magnetic suppression structures for our tests can not keep the plasma back enough. A reduced effective port (a slit or aperture) size and/or a fine metal mesh may be needed. If using reduced ports, plasma region that can be diagnosed will be affected. If using a metal mesh, grid size should be small, as Debye length at the plasma edge is approximately 0.1mm.

Our conclusion about this issue is: Plasma loading effect is large, and some kind of modified magnetic suppression structures for both entrance and exit ports are needed. This will somehow compromise our measurement range on the MST. Whether or not the suppression structures that will be used allow us to scan through the whole angular range that has been designed for the sweep system is still an open issue. UV loading effect hasn't been addressed in our sweep plates tests, so this effect may not be negligible on the sweep plates. Whether UV will influence our modified energy analyzer's behavior is still an open issue.

5.5 Beam modulation, path effect and false potential fluctuation signals

To determine the secondary current at the detector, one has to calculate the attenuation of the primary beam and secondary beam in the plasma. The current detected is given by [44]:

$$I_{ds} = 2\kappa I_{prim}\sigma_s^{1\to 2}\lambda_s n_s exp\left\{-\int_{P1}^{SV} n_e(\rho)\sigma^1(\rho)dl - \int_{SV}^{P2} n_e(\rho)\sigma^2(\rho)dl\right\} \tag{13}$$

where I_{ds} is the detected sum signal, κ the secondary emission coefficient, I_{prim} the primary beam current, $\sigma_s^{1\to 2}$ is the effective cross section for 1+ to 2+ electron impact ionization, λ_s is the sample volume's thickness, n_s the electron density at the sample volume, $n_e(\rho)$ the electron density, σ^1 and σ^2 are effective primary and secondary attenuation cross sections, $P1$ and $P2$ are points where the beam enters and exits the plasma, SV the sample volume. From the above equation, we can see that fluctuations in the plasma density and electron temperature along the trajectory contribute to the sum signal fluctuations in addition to the 'true' signal generated by fluctuations at the sample volume. This has been refered to as a beam modulation and/or a path effect. If we neglect temperature fluctuation effects, the

normalized current fluctuation signal is [34]

$$\frac{\tilde{I}_s}{I_s^0} = \frac{\tilde{n}_e}{n_e} - \int_{P1}^{SV} \sigma^1 \tilde{n}_e dl - \int_{SV}^{P2} \sigma^2 \tilde{n}_e dl \tag{14}$$

Upper bounds on the path effect can be estimated by using experimental density and temperature profiles. The beam modulation effect is of particular interest in studying the interior fluctuations. The conclusion of the TEXT simulations is that the modulation effects are present and probably affecting the signals, but not by a large factor [36] [45]. But these effects have to be examined for the MST HIBP.

It has been noticed that a density fluctuation can yield a false potential fluctuation signal, especially when the component of wavenumber normal to the sample disk face is close to $2\pi/\lambda_s$, where λ_s is the thickness of the sample volume disk. In practice, typical wavelengths are much larger than the short dimension of the sample volume ($\sim 1mm$). If we assume $\tilde{n}/n \ll 1$, the false potential fluctuation signal can be estimated as: [36]

$$\tilde{\phi}_{false} = -\frac{j}{2} C \frac{\tilde{n}}{n} kd$$

where d is the width of the sample volume, $C = q_s V_A F(\theta_I, \alpha)/(q_s - q_p)$, and j indicates 90° out of phase. This effect can be corrected by taking measurements with several different slit openings. The effect can be reduced by reducing the entrance slit opening, too. In the TEXT HIBP, this effect is significant. In the MST HIBP, this effect is yet to be studied.

5.6 Wavenumber measurement issue

The fluctuating electric field is derived according to $\tilde{E} = -i\bar{k}\tilde{\phi}$, where $\bar{k}$ is the average wavenumber. The wavenumber is given by ratio of phase shift and distance between two

nearby sample volumes. In principle, the phase shift is undetermined because you can add $2\pi m$ to the shift where m is any integer without changing the signal. However, in practice, it is usually possible to determine the integer with reasonable assumptions [36]. The sample volume separation should be smaller than the correlation length l_c in order for the wavenumber measurement to make sense.

In previous HIBPs, the separation of the two sample volumes is a function of initial injection position, injection angle, magnetic field distribution in the plasma, position of the analyzer, and separation of the two nearby entrance slits. In the MST HIBP, things become a little bit complicated as there are secondary sweep plates in the secondary beamline. Some kinds of effective entrance slits are needed to be mapped to the front of the sweep plates. We don't have a proper simulation program taking care of this situation at present. I propose to make a computer simulation program to address this issue. The program should follow the outline below:

A. Find a primary ion trajectory which has a section from where secondary ions can reach the front of the secondary sweep system. Let's call this section as 'target section'. If this fails, change the injection conditions and redo this process.

B. From this 'target section', find a point from where the secondary ions can be steered into the energy analyzer's one entrance slit with certain voltages applied to the secondary sweep plates. Let's call this point as '1st target point', voltages applied as '1st tried voltages', and entrance slit as '1st slit'. If this fails, go back and repeat from process A.

C. With fixed '1st tried voltages', look for another point on the 'target section' from where the secondary ions can reach energy analyzer's entrance slit next to the '1st slit'. Let's call this point as '2nd target point'. If this fails, go back and repeat from process A.

D. Iterate through $A \rightarrow C$ until we can find both 1st and 2nd 'target points'.

Another issue in wavenumber measurement is its direction. In previous HIBPs, wavenumbers primarily in the poloidal direction were usually measured, with assumption that the perpendicular motion of the modes is poloidally dominated. In the MST, as $q < 1$ because of comparable poloidal and toroidal magnetic field, modes will be more in helical direction. We have to take a look at this once secondary signals been detected.

References

[1] H.A.B. Bodin and A.A. Newton, *REVIEW PAPER, REVERSED-FIELD-PINCH RESEARCH*, Nucl. Fusion Vol.20, No.10, 1980, pp.1255-1324

[2] H.A.B. Bodin, *The Reversed Field Pinch*, Nuclear Fusion, vol 30, No .9, 1990, pp.1717-1737

[3] The TITAN Reversed-Field-inch Fusion Reactor Study, Final Report, report UCLA-PPG-1200, University of California-Los Angeles (1990)

[4] The Reversed Field Pinch, A proposal for RFP Research in the U.S., Prepared by Members of the U.S. RFP Research Community, May, 1998

[5] W. Shen *Measurement of Current Density Fluctuations and Ambipolar Particle Flux Due to Magnetic Fluctuations in MST* Ph. D Thesis, Aug. 1992

[6] A Proposal to U.S. Department of Energy Research Office of Fusion Energy Sciences For Reversed Field Pinch Research in MST, Nov. 1,1998-Oct. 31,2001

[7] P. C. Liewer, *Measurements of Microturbulence in Tokamaks and Comparisons with Theories of Turbulence and Anomalous Transport* Nuclear Fusion, Vol. 25, No. 5, (1985), P. 543

[8] F. C. Jobes and R. L. Hickok, *A direct measurement of plasma space potential*, Nucl. fusion, vol. 10, pp. 195-197, 1970

[9] G. A. Hallock *et al.*, *Space potential distribution in the ISX-B tokamak*, Phys. Rev. Lett. vol. 56, pp.1248-1251, 1986

[10] J. C. Foster, *Study of density and space potential fluctuations on the TEXT tokamak using a heavy ion beam probe*, Ph. D. thesis, RPI, 1987

[11] G. A. Hallock, *Space-potential and density Fluctuations in the ISX-B Tokamak*, Phys. Rev. Lett. V59, No. 12, Sep 1987, P1301

[12] J. Schwelberger, *Measurement of the poloidal magnetic flux in the TEXT tokamak using a heavy ion beam probe*, Ph. D. thesis, RPI, 1994

[13] J. C. Foster, *Study of Density and Potential Fluctuations in the TEXT Tokamak with a Heavy Ion Beam Probe*, IEEE Trans. Plasma Science, Vol. 22, No. 4, Aug. 1994, P.359

[14] J. Schwelberger, et al., *Electron density profile measurements with a heavy ion beam probe*, RSI, 63, 4571-4573, Oct., 1992

[15] J. W. Heard, *Broadband density fluctuation measurement using a heavy ion beam probe on the Texas Experimental Tokamak*, Phys. Plasma, 2 (9), Sep. 1995, P.3360

[16] P. M. Schoch, R. L. Hickok, and W. C. Jennings, *Comparition of the radial profile measured in a tokamak to predictions of stochastic magnetic field theory*, Phys. Rev. Lett., vol. 55, pp. 2417-2420, 1985

[17] J. R. Goyer, K. A. Connor and R. L. Hickok, *Temperature and Density Measurements in a Non-Axisymmetric, Continuously Operating Fusion Experiment Using a Heavy Ion Beam Probe*, IEEE Trans. Plasma Science, Vol. 22, No. 4, Aug. 1994, P.403

[18] V. J. Simcic, et al., *MHD Magnetic Fluctuation Measurements using a heavy ion beam probe*, Rev. Sci, Instrum., vol, 61, pp. 3061-3063

[19] E. J. Powers, *Spectral techniques for experimental investigation of plasma diffusion due to polychromatic fluctuations*, Nicl. Fusion, vol. 14, pp. 749-752, 1974

[20] K. Itoh, et al., *Roles of Electric Field on Toroidal Magnetic Confinement*, IEEE Trans. Plasma Science, Vol. 22, No.4, Aug. 1994

[21] G. Fiksel, et al., *Measurement of Magnetic Fluctuation -induced heat Transport in Tokamaks and RFP*, Plasma Phys. Control Fusion 38 (1996) A213

[22] B. E. Chapman, et al., *ExB Flow Shear and Enhanced Confinement in the Madison Symmetric Torus Reversed-Field Pinch*, Invited talk at the 39th Annual Meeting, APS division of Plasma Physics. Nov., 1997, Pittsburgh, PA.

[23] Uday Shah, *Design of a Heavy Ion Beam Probe for the Madison Symmetric Torus*, RSI special issue for the 20th high temperature plasma diagnostic conference, Princeton, June, 1998

[24] Joe Mathew, Ph. D thesis, RPI, 1984

[25] L. Solensten and K. A. Connor, *Heavy ion beam probe energy analyzer for measurement of plasma potential fluctuations*, Rev. Sci. Instrum., vol. 58, no. 4, pp. 516-519, 1987

[26] T. D. Rempel, et al., *Edge Electrostatic Fluctuations and Transport in a Reversed-Field Pinch*, Phys. Rev. Lett., Vol. 67, No. 11, Sep. 1991, P.1438

[27] D. J. Hartog, et al., *Measurement of core velocity fluctuations and the dynamo in a reversed-field pinch*, Phys. Fluids, vol. 6, no. 5, pp.1813-1821, May, 1991

[28] Den J. Hartog, et al., *Velocity fluctuations Measurement with IDS in MST*, MST Report, 1999

[29] Y. Jiang, et al., *Electron Density Fluctuation Characteristics During Enhanced Confinement in MST*, Poster at the 40th Annual Meeting, APS, New Orleans, LA,1998

[30] N. Crocker, et al., 1997

[31] A. J. Wooton, et al., *Fluctuations and anomalous transport in tokamaks*, Phys. Fluids B, 2 (12), Dec. 1990, pp. 2879-2903

[32] J. B. Taylor, , Rev. Mod. Phys., 58, 741, 1986

[33] J. Lei, et al., *Sweep plates design for the MST HIBP*, RSI special issue for the 20th high temperature plasma diagnostic conference, Princeton, June, 1998

[34] J. W. Heard, *Anomalous Transport Measurements Using a Heavy Ion Beam Probe on the TEXT Tokamak*, Ph. D. thesis, RPI, 1994

[35] A. Ouroua, et. al., *Measurements of Broadband fluctuations and plasma potential with the 2 MeV heavy ion beam probe on the TEXT-U Tokamak*, Fusion Engineering and Design, 34-35 (1997) 613-616

[36] T. P. Crowley, *Rensselaer Heavy ion Beam Probe Diagnostic Methods and Techniques*, IEEE Tran. on Plasma Sci., vol. 22, No. 4, Aug. 1994, pp. 291-309

[37] J. T. Chapman, *Spectroscopic Measurement of the MHD Dynamo in the Reversed Field Pinch*, Ph. D Thesis, Univ. Wisconsin, Sep. 1998

[38] S. Aceto, Ph. D. thesis, RPI, 1994

[39] T.T. Tang, *Introduction to Charged Paricle Optics*, XJTU Press, 1986

[40] http://hibp.ecse.rpi.edu/msthibp/report.ps 'or' report.pdf

[41] http://www.public.iastate.edu/ rpolikar/WAVELETS/WTtutorial.html

[42] http://hibp.ecse.rpi.edu/msthibp/PBD.html

[43] Uday Shah, *Proposal for the measurement of the radial electric field on the Madison Symmetric Torus*, thesis proposal, June, 1998

[44] J. G. Schwelberger and K. A. Connor, *Atomic Collision Processes Relevant for Heavy Ion Beam Probes*, IEEE Trans. Plasma Science, vol 22, No. 4, Aug, 1994, pp.418-423

[45] J. W. Heard, et al., *Path Integral effects in heavy ion beam probe density measurements: A comparision of simulation results and experimental data*, RSI, 64 (4), Apr. 1993